High rectifying behavior in Al/Sinanocrystal-embedded SiOxNy/p-Si heterojunctions

Emmanuel Jacques, Laurent Pichon, Olivier Debieu, Fabrice Gourbilleau, Nathalie Coulon

High rectifying behavior in Al/Si nanocrystal-embedded SiO_xN_y/p-Si heterojunctions

2011 Semicond. Sci. Technol. 26 055005

(http://iopscience.iop.org/0268-1242/26/5/055005)

Semicond. Sci. Technol. **26** (2011) 055005 (5pp) doi:10.1088/0268-1242/26/5/055005

High rectifying behavior in Al/Si nanocrystal-embedded SiO_xN_y/p-Si heterojunctions

E Jacques[1], L Pichon[1], O Debieu[2], F Gourbilleau[2] and N Coulon[1]

[1] Groupe Microélectronique, IETR, UMR CNRS 6164, Campus de Beaulieu, 35042 Rennes Cedex, France
[2] Centre de Recherche sur les Ions, les Matériaux et la Photonique, CEA, UMR CNRS, ENSICAEN, 6 Boulevard du Maréchal Juin, 14050 Caen Cedex 4, France

E-mail: emmanuel.jacques@univ-rennes1.fr

Received 27 May 2010, in final form 3 December 2010
Published 11 March 2011
Online at stacks.iop.org/SST/26/055005

Abstract
We examine the electrical properties of MIS devices made of Al/Si nanocrystal–SiO_xN_y/p-Si. The *J*–*V* characteristics of the devices present a high rectifying behavior. Temperature measurements show that the forward current is thermally activated following the thermal diffusion model of carriers. At low reverse bias, the current is governed by thermal emission amplified by the Poole–Frenkel effect of carriers from defects located at the silicon nanocrystals/SiO_xN_y interfaces, whereas tunnel conduction in silicon oxynitride matrix dominates at high reverse bias. The devices exhibit a rectification ratio $>10^4$ for the current measured at $V = \pm 1$ V. Study reveals that thermal annealing in forming gas (H_2/N_2) improves the electrical properties of the devices due to the passivation of defects.

1. Introduction

Silicon heterojunctions have been extensively studied for understanding the physics of the device as well as their applications to majority carrier rectifiers [1], photodetectors [2], solar cells [3] and indirect gap injection lasers [4]. Because of its indirect bandgap, silicon is a highly inefficient material for a light emitter. However, to overcome this problem different approaches were developed in this last decade for the fabrication of Si-based light emitting sources made of silicon nanocrystals (nc-Si) embedded in SiO_2 matrix.

Due to quantum confinement effects, nc-Si are characterized by an energy band gap which is enlarged with respect to bulk silicon and an intense room temperature photoluminescence can be obtained in the visible–near-infrared (IR) range [5–9]. However, photoluminescence in silica matrix is affected by the choice of the annealing environment (Ar or H_2). In particular, a previous study [10] recently reported that the presence of incorporated nitrogen species influences the nc-Si growth and affects the photoluminescence in a SiO_xN_y–nc-Si layer. In addition, the IR emission properties were also reported in matrix embedding nc-Si and rare-earth ions. In such a system, the emitting rare-earth ions benefit from the quantum confinement properties of the carriers in nc-Si to be efficiently excited by an energy transfer mechanism within the silica matrix. Previous studies reported IR light emission at 1.54 and 1.06 μm in silica matrix respectively incorporating erbium or neodymium [11–14]. Electroluminescence in SiO_xN_y–nc-Si-based IR light-emitting devices is limited by the difficulty in carrier injection. Therefore, prior to developing IR light-emitting devices a good understanding for optimum carrier injection in SiO_xN_y–nc-Si-type layers is needed. In this way, previous works have been recently reported on electrical properties in MIS devices fabricated with such silicon-rich oxide layers either deposited by (i) a PECVD (plasma-enhanced chemical vapor deposition) technique [15] or by (ii) magnetron co-sputtering of Si, SiO_2 [16]. In the first case, rectifying behavior was observed, whereas in the second one it was not observed. In addition, the thermal dependence of the carrier transport was not studied.

In this work, we report a detailed study of the carrier transport governing electrical properties in Al/SiO_xN_y–nc-Si/p-Si heterojunctions exhibiting a high rectifying behavior.

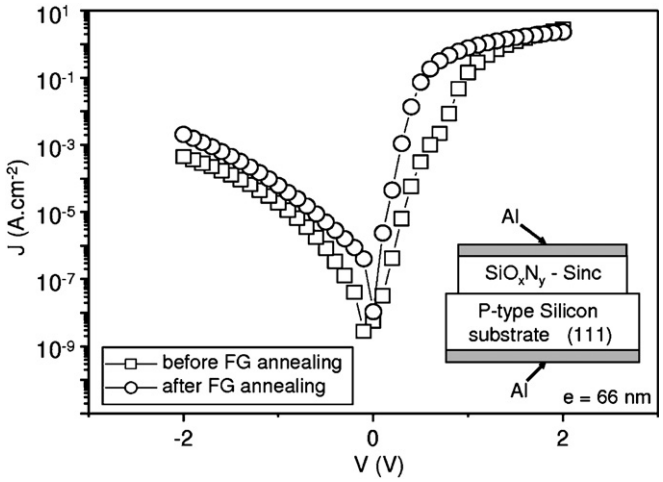

Figure 1. Effects of the thermal annealing in forming gas (H_2:N_2, 10%) on the current density–voltage characteristics plotted in semilog scale. Inset: schematic cross section of the tested Al/SiO_xN_y–nc-Si/p-Si structures.

The devices are fabricated with nc-Si embedded in a SiO_xN_y layer deposited by reactive magnetron sputtering of a pure SiO_2 cathode. The thermal and the bias dependences of the carrier transport are analyzed.

2. Device technology and experimental details

Devices are elaborated on p-type (1 1 1) oriented silicon substrates with resistivity in the range of 0.001–0.005 Ω cm (boron doping level 2–8 $\times$ 10^{19} cm^{-3}). SiO_xN_y–nc-Si layers 31 and 66 nm thick, respectively, were deposited by reactive magnetron sputtering of pure SiO_2 target, under a mixture of $H_2/Ar/N_2$-rich plasma [17]. After deposition, the films were submitted to thermal annealing at 900 °C for 30 min under N_2 flux. Next, aluminum was thermally evaporated on a SiO_xN_y–nc-Si layer. Both aluminum and SiO_xN_y–nc-Si layers were patterned by wet etching to define the geometry of the device. A second thermal evaporation of aluminum on the back surface was carried out to ensure ohmic contact with the p-type crystalline silicon (see the inset of figure 1). Finally, the devices were annealed in forming gas (H_2:N_2, 10%) at 390 °C during an optimum duration of 30 min to stabilize the electrical properties of the devices.

Static electrical characteristics $J(V)$ are collected by using an HP 4155 B semiconductor parameter analyzer. For temperature measurements from 203 to 503 K samples are placed in a cryostat under vacuum (10^{-5}–10^{-4} Pa). All measurements were made in darkness on more than 20 devices homogeneously located over the 2 inch surface substrate. The area of each tested device is 0.32 mm^2.

3. Results and discussion

The high rectifying behavior of the J–V characteristics of the devices plotted in figure 1, for a 66 nm thick layer, shows that the SiO_xN_y–nc-Si layer is n-type doped. This can be explained by the presence of the incorporated nitrogen (15 at.%) during the fabrication process of these layers, acting as n-type doping species in silicon films [18], and thus also in silicon-rich oxynitride layers. In this case, at low forward bias (0 V $\leqslant V \leqslant$ 0.8 V), current density taking account of serial resistance can be described by

$$J = J_0 \left(\exp \frac{qV - RJ}{nk_BT} - 1 \right), \quad (1)$$

where q is the electron charge, k_B the Boltzmann constant, n the ideality factor dealing with current dominated by carrier diffusion ($n = 1$) and/or by carrier recombination processes at defects ($n = 2$), R the global serial resistance, and J_0 the saturation current density estimated to be $\sim 2 \times 10^{-9}$ A cm^{-2} at 293 K. The ideality factor n and serial resistance R are deduced by fitting our experimental results with the theoretical model (1). The thermal annealing effect in forming gas on the electrical properties of the devices is displayed as the $J(V)$ characteristics (figure 1). Before annealing $1 \leqslant n \leqslant 2$ indicating a conduction due to a mix of diffusion and recombination processes of carriers, whereas after annealing $n \approx 1.2$ for the 66 nm thick layer indicating domination of carrier diffusion and $n \approx 2$ for the 31 nm thick indicating domination of the recombination mechanism. The decrease of n for the device made with a 66 nm thick SiO_xN_y–nc-Si layer suggests that thermal annealing in forming gas would induce some hydrogen redistribution within the SiO_xN_y–nc-Si matrix and/or both at the Al/SiO_xN_y–nc-Si and Al/p-Si interfaces, and thus the possible recovery of the defects. This phenomenon would lead to the reduction of the defect density responsible for conduction due to carrier recombination. In the case of the device made with a 31 nm thick SiO_xN_y–nc-Si layer this phenomenon does not occur likely due to a higher defect density, as it will be further discussed. However, $J(V)$ plots of each annealed device have an excellent rectifying ratio ($>10^4$ for current measured at $V = \pm$ 1 V) leading to a much higher injected current level than obtained in others works [8, 19, 20]. This result is promising for the electroluminescent properties of the device. Indeed, a high level current in the forward mode is strongly related to the high confinement of the carriers in nc-Si to efficiently excite rare-earth species thanks to energy transfer within the silica matrix. In addition, at high voltages (2 V $> V >$ 0.8 V) current deviates from the exponential behavior due to the low serial resistance for both devices. These serial resistances were estimated in the range 20 Ω $\leqslant R \leqslant$ 40 Ω. All these results, summed up in table 1, show a high rectifying behavior of the devices related to a high carrier injection into the SiO_xN_y–nc-Si layer.

The electrical behavior of the annealed device made either with 31 nm or 66 nm thick SiO_xN_y–nc-Si layer is similar in the forward mode, whereas some differences appear in the reverse mode. The higher current level measured in the reverse mode (-2 V $\leqslant V \leqslant$ 0 V) for the annealed device can be explained by a decrease of the carrier trapping effect at the defects located at the SiO_xN_y–nc-Si /p-Si interface leading to a lower barrier energy at this interface.

For annealed devices, analysis of the electrical properties is then carried out according to the carrier's temperature dependence. Temperature measurements do not affect the

Table 1. Summary of the thermal annealing effects on the electrical parameters of the MIS structures.

	Before annealing in forming gas	After annealing in forming gas
Ideality factor	$1 \leqslant n \leqslant 2$	1, 2 ($e = 66$ nm) 2 ($e = 31$ nm)
Rectifying ratio at $V \pm 1$V	7×10^3	5×10^4
Series resistance (Ω)	$20 \leqslant R \leqslant 40$	$20 \leqslant R \leqslant 40$

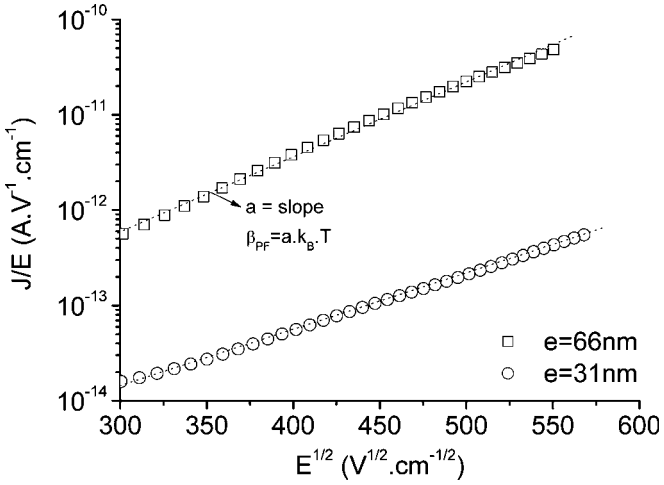

Figure 2. Plots of $\ln(J/E)$ versus $E^{1/2}$ of the two types of Al/SiO_xN_y–nc-Si/p-Si structures.

benefit of the thermal annealing effect on the electrical behavior of the structures. First, for the forward mode, the ideality factor n and the saturation current density J_0 have been estimated for a range of temperature about 203 K $\leqslant T \leqslant$ 503 K. When the temperature increases, it has been verified that n decreases for both devices to a lower value $n = 1$ and that J_0 increases to 2×10^{-8} A cm^{-2}. These behaviors are in accordance with the classical increase of the diffusion process as the temperature increases [21]. In the reverse mode, the Poole–Frenkel (PF) model is the best convenience. In this model, electrons are thermally emitted from the randomly distributed traps to the conduction band as a result of the lowering of the columbic potential barrier by an external electric field. This model is represented by the following relation [22]:

$$J = N\mu E \exp\left(-\frac{\phi_0}{k_B T}\right) \exp\left(\frac{\beta_{PF} E^{1/2}}{k_B T}\right), \qquad (2)$$

where J is the current density, N the density of trapping sites, μ the effective carrier mobility, E the local electric field, Φ_0 the zero-field trap energy barrier depth and β_{PF} the PF coefficient.

Assuming that E is mainly due to the reverse bias V (i.e. $E \approx V/d$, with d being the SiO_xN_y–nc-Si layer thickness), we have extracted the PF coefficient obtained with the slope rate value from the linear representation of $\ln(J/E) = f(E^{1/2})$ shown in figure 2. The linear part corresponds to the validity range of the PF model that begins for the electric field from 300 V cm^{-1} ($V < -0,2$ V). The slight difference between the two slope rates is related to the permittivity difference of the two studied SiO_xN_y–nc-Si layers. The permittivity (ε_r) is deduced from the PF coefficient according to

$$\beta_{PF} = \left(\frac{q^3}{\pi \varepsilon_0 \varepsilon_r}\right)^{1/2}. \qquad (3)$$

The corresponding values are $\varepsilon_r = 5.6$ and $\varepsilon_r = 4.4$ for the 31 nm and the 66 nm thick SiO_xN_y–nc-Si layers, respectively, and they are characteristics of a modification of the layer composition. Among the possible hypotheses that may arise to explain this difference for ε_r values two are: (i) a change of the density of nc-Si (for the same Si content) with the thickness and (ii) a change in the Si content. These suggest that during the first step of the deposition process, the starting growth process conditions could promote the deposition of Si within a few nanometers thickness due to the vicinity of the Si substrate. This idea is strengthened by the increase of the refractive index from 1.61 to 1.75 when the thickness was reduced. The increase of the Si content would result in a higher nc-Si density for the thinnest SiO_xN_y–nc-Si layers. This assumption could be related to a higher fraction of clustered silicon, as observed in the thinnest sputter-deposited SiO_x layers for thicknesses lower than 150 nm [23]. Quasi-static C–V measurements have been made to check the validity of the obtained permittivity values. Several samples have been tested and give respectively the average values of $\varepsilon_r = 5.1$ and $\varepsilon_r = 4.3$ for the 31 and 66 nm thicknesses.

In the PF model, the current is thermally activated and the corresponding activation energy, E_a, is defined by the following relation:

$$E_a = \phi_0 - \beta_{PF} E^{1/2}. \qquad (4)$$

In this way, temperature measurements of the current have been carried out and Arrhenius diagrams of $\ln(J)$ versus $1/T$ are presented in figures 3(a) and (b) respectively for the two thicknesses $e = 31$ nm and $e = 66$ nm. The linear decrease of the curves ($T > 383$ K) shows that conduction is thermally activated. The corresponding activation energy has been extracted for several polarization points in the reverse mode. The dependence of E_a on $E^{1/2}$ (see figure 4(a)) for the two types of devices corresponds to relation (4). In addition, the values of the measured activation energies are lower compared to the values required for emission of carriers from defects located into insulating films. Therefore, we suggest that the PF mechanism should take place at defects located at the nc-Si/SiO_xN_y interfaces (see figure 4(b)). This could be related to induction of interface traps, usually observed under bias stress in MOS devices, and responsible for the emission of carriers. These interface traps could come from unsatisfied bonds (dangling bonds) at the nc-Si/SiO_xN_y interfaces. Most Si atoms are bonded to oxygen while some are bonded with residual nitrogen or hydrogen content due to plasma mixture during the deposition of SiO_xN_y layers. Because under bias stress some Si–H bonds break, the interface trap is then a trivalent Si atom with an unsaturated valence electron at the SiO_x/Si interface [24]. Moreover, the lower measured activation energy for devices made with a 66 nm thick SiO_xN_y–nc-Si layer could be explained by the nitrogen doping level

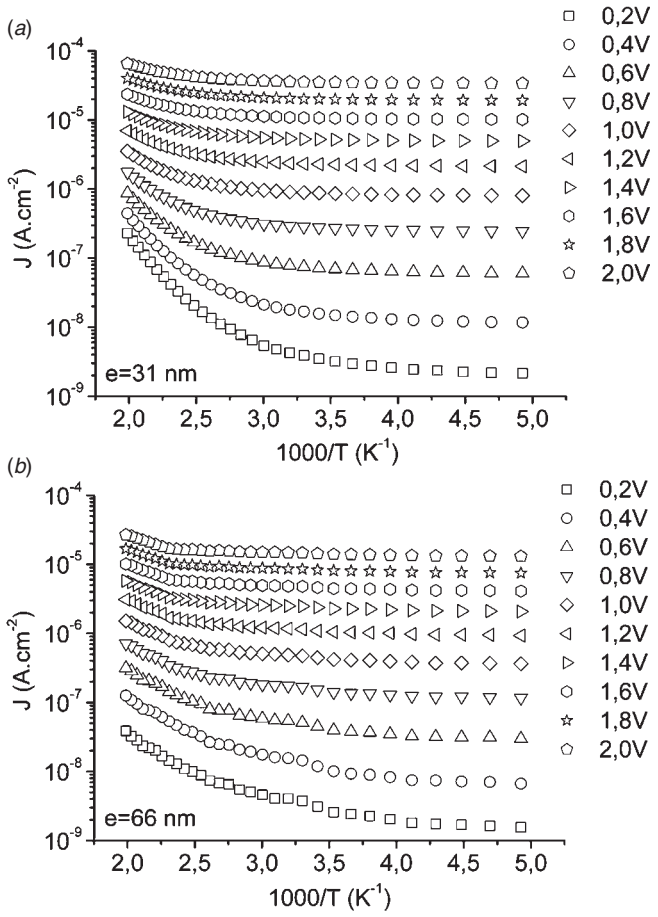

Figure 3. Arrhenius representations of the current density of the MIS structures made with 31 nm (*a*) and 66 nm (*b*) thick SiO_xN_y–nc-Si layers.

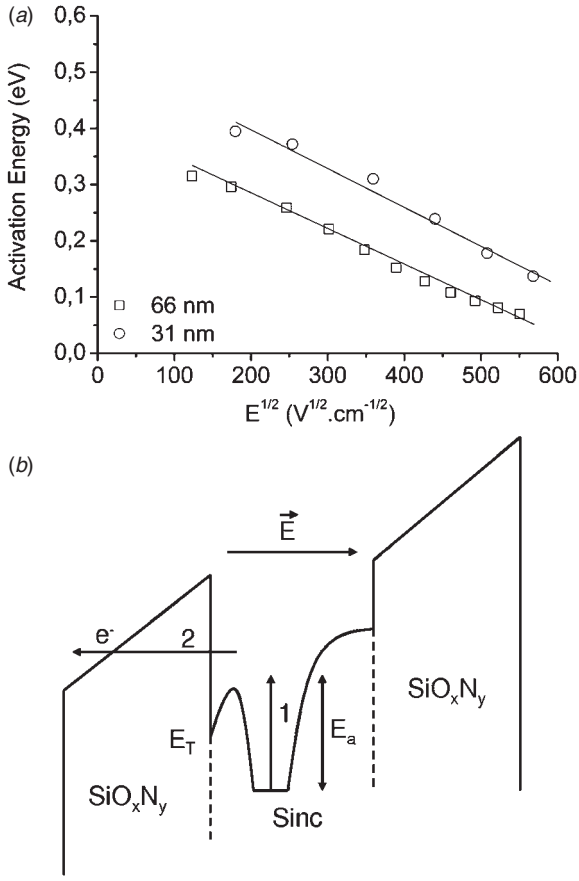

Figure 4. (*a*) Variations of the activation energy versus the electric field square roots. (*b*) Schematic band diagram describing the proposed conduction mechanisms in the MIS structures: process (1), PF thermal emission; process (2), tunnel effect.

effect. Indeed, the 15 at.% nitrogen content incorporated during deposition of the SiO_xN_y–nc-Si layer, embedding a lower nc-Si density, could produce a higher doping effect. In this case, because emission of electrons occurs from the trap level (E_T) located close to the Fermi level (E_F), a higher doping effect corresponding to a higher level E_F in the nc-Si would give lower activation energy.

For low temperature ($T \leqslant 373$ K) the current does not depend on the temperature indicating that it is more representative of a tunnel conduction way. This behavior is more pronounced at high reverse bias, and it is effective between the adjacent nc-Si through the silicon oxynitride [20]. In addition, for the devices made with a 66 nm thick SiO_xN_y–nc-Si layer, with a suspected lower density of nc-Si, this tunnel effect is then higher for a higher range of temperature. From these results, we can conclude that the conduction in the reverse mode is due to a mix of PF and tunnel mechanisms.

These results lead to the conclusion that the conduction in the reverse mode through the SiO_xN_y–nc-Si layer, associated with the thermal generation of carriers from defects at the interface SiO_xN_y/nc-Si, is related to the nc-Si density. This is consistent with the ideality factor close to 2 measured by direct injection for devices fabricated with the thinnest SiO_xN_y–nc-Si layer (31 nm) embedding a suspected higher nc-Si density.

4. Conclusion

The use of a SiO_xN_y–nc-Si layer to achieve diodes with a high rectifying ratio has been validated. The high rectifying ratio comes from the presence of nitrogen in the layer that plays the role of n-type doping species. Our analysis shows that the electrical properties of these diodes are strongly dependent on the defects within the SiO_xN_y–nc-Si layer. In the forward mode, the rectifying behavior is enhanced due to a likely decrease of defect density after thermal annealing. In addition, the study of a reverse regime shows a mix of PF emission from defects located at the nc-Si/SiO_xN_y interfaces and a tunnel mechanism that could occur between adjacent nanocrystals embedded in the silicon oxynitride matrix.

These structures with a high rectifying ratio are very promising for high electrical injection in the nc-Si and therefore interesting for an energy transfer to the rare earth ions for an IR emission. The next step of this study will consist in analyzing the coupling of nc-Si rare earth ions on the electroluminescence phenomenon in the case of electrical pumping.

Acknowledgment

This work was financially supported by the Agence National de la Recherche (France) through the program PNANO-ANR-08-NANO-005 entitled DAPHNES (Dispositifs Appliqués à la Photonique à base de Néodyme et de Silicium).

References

[1] Matsuura H, Okuno T, Okushi H and Tanaka K 1984 *J. Appl. Phys.* **55** 1012
[2] Zhang T C, Guo Y, Mei Z X, Gu C Z and Du X L 2009 *Appl. Phys. Lett.* **94** 113508
[3] Xu Y, Hu Z, Diao H, Cai Y, Zhang S, Zeng X, Hao H, Liao X, Fortunato E and Martins R 2006 *J. Non-Cryst. Solids* **352** 1972
[4] Marinace J C 1960 *IBM J. Res. Dev.* **4** 280
[5] Min K S, Shcheglov K V, Yang C M, Atwater H A, Brongersma M L and Polman A 1996 *Appl. Phys. Lett.* **69** 2033
[6] Franzò G, Miritello M, Boninelli S, Lo Savio R, Grimaldi M G, Priolo F, Iacona F, Nicotra G, Spinella C and Coffa S 2008 *J. Appl. Phys.* **104** 094306
[7] Kenyon A J, Trwoga P F, Federighi M and Pitt C W 1994 *J. Phys.: Condens. Matter* **6** L319
[8] Pellegrino P, Garrido B, Arbiol J, García C, Lebour Y and Morante J R 2006 *Appl. Phys. Lett.* **88** 121915
[9] Gourbilleau F, Levallois M, Dufour C, Vicens J and Rizk R 2004 *J. Appl. Phys.* **95** 3717
[10] Bolduc M, Genard G, Yedji M, Barba D, Martin F, Terwagne G and Ross G G 2009 *J. Appl. Phys.* **105** 013108
[11] Priolo F, Franzo G, Pacifici D, Vinciguerra V, Iacona F and Irrera A 2001 *J. Appl. Phys.* **89** 264
[12] Irrera A, Iacona F, Franzo G, Miritello M, Lo Savio R, Castagna M E, Coffa S and Priolo F 2010 *J. Appl. Phys.* **107** 054302
[13] Seo S-Y, Kim M-J and Shin J 2003 *Appl. Phys. Lett.* **83** 2778
[14] Gourbilleau F, Khomenkova L, Breard D, Dufour C and Rizk R 2009 *Physica* E **41** 1034
[15] Prezioso S, Anopchenko A, Gaburro Z, Pavesi L, Pucker G, Vanzetti L and Bellutti P 2008 *J. Appl. Phys.* **104** 063103
[16] Jambois O, Berencen Y, Hijazi K, Wojdak M, Kenyon A J, Gourbilleau F, Rizk R and Garrido B 2009 *J. Appl. Phys.* **106** 063526
[17] Ternon C, Gourbilleau F, Portier X, Voivenet P and Dufour C 2002 *Thin Solid Films* **419** 5
[18] Temple-Boyer P, Jalabert L, Couderc E, Scheid E, Fadel P and Rousset B 2002 *Thin Solid Films* **414** 13
[19] Anopchenko A, Marconi A, Moser E, Prezioso S, Wang M, Pavesi L, Pucker G and Bellutti P 2009 *J. Appl. Phys.* **106** 033104
[20] Wong J I, Chen T P, Yang M, Liu Y, Ng C Y and Ding L 2009 *J. Appl. Phys.* **106** 013718
[21] Sze S M 1981 *Physics of Semiconductor Devices* (New York: Wiley)
[22] Harnell W R and Frey J 1999 *Thin Solid Films* **352** 195
[23] Cueff S, Labbe C, Cardin J, Hijazi K, Doualan J L, Jambois O, Garrido B and Rizk R 2010 *Phys. Status Solidi* at press
[24] Schroder D K and Babcock J A 2003 *Appl. Phys. Rev.* **94** 1